Mine Water and the Environment (2024) 43:28–40
https://doi.org/10.1007/s10230-023-00963-1

TECHNICAL ARTICLE

Hydrogeochemical Mechanisms and Hydraulic Connection of Groundwaters in the Dongming Opencast Coal Mine, Hailar, Inner Mongolia

Xiaoyong Zhong[1] · Qiang Wu[1,2] · Bo Tang[3] · Yunchuan Wang[3] · Junbin Chen[3] · Yifan Zeng[1,2]

Received: 17 April 2023 / Accepted: 2 November 2023 / Published online: 3 January 2024

Abstract

The identification of water sources and hydraulic connectivity in different aquifers within coal mines is crucial for effective groundwater management and has important implications for mine safety, water resource conservation, and regional ecological protection. The Dongming opencast coal mine in Hailar City, Inner Mongolia, China, is threatened by groundwater leakage. However, the hydrochemical mechanisms, water sources, and hydraulic connectivity of the different aquifers in this area are still not well understood. In this study, we collected 24 samples from various water sources, including pore water in the Quaternary aquifer (QGW), pore-fissure water in the coal-bearing aquifer (CGW), drainage sump water from the mine pit (DSW), Morigele river water (MRW), and nearby snow water (SNW). These samples were analyzed for major and trace elements, as well as hydrogen (H), oxygen (O), and boron (B) isotope compositions. The results showed that the QGW and MRW hydrochemistry were similar, while the CGW and DSW had comparable characteristics. The H and O isotope analyses revealed that all of the groundwater samples originated from river water, while the B isotope analyses indicated the heterogeneous hydraulic connectivity between the different aquifers and the river. The research findings indicate that mining companies should continuously strengthen the monitoring of surface water and groundwater levels, further investigate the velocity and direction of groundwater flow, and gradually conduct quantitative research on hydraulic connections between surface water and different aquifers. This will provide more scientific basis for the prevention and control of groundwater leakage in mining areas. In this study, a combination of hydrochemical and non-traditional stable isotope geochemical methods was used to investigate the origin of groundwater in open-pit coal mines and its relationship with different water bodies. This represents a new exploration of research ideas and methods. This work has important implications for the study of the origin of groundwater and the measures for leakage prevention and control in open-pit coal mines and underground coal mines worldwide.

Keywords Solute sources · Salinization mechanism · H–O–B isotopes · Leakage controlling

Introduction

Coal plays a crucial role in China's energy supply. The coal-bearing strata in the country are typically accompanied by abundant groundwater resources. In recent years, there has been a growing focus on the environmentally friendly groundwater management during coal mining. This includes controlling groundwater discharges, utilizing water resources comprehensively, and maintaining groundwater levels (Gu et al. 2021; Huang et al. 2022; Tarasenko et al. 2022; Zhao et al. 2017, 2022). Effectively managing groundwater requires identifying the main aquifers and

✉ Qiang Wu
wuq@cumtb.edu.cn

[1] National Engineering Research Center of Coal Mine Water Hazard Controlling, China University of Mining and Technology, Beijing 100083, China

[2] Mine Water Hazard Prevention National Mine Safety Administration Key Laboratory, Beijing 100083, China

[3] Dongming Opencast Coal Mine, Hailar 021000, Inner Mongolia, China

understanding the hydraulic connection between different aquifers. However, traditional hydrogeological investigations face challenges in accurately determining hydraulic connections, recharge flux, and groundwater hydrochemical field connections in coal-bearing strata. These challenges arise from the uneven distribution and limited number of hydrogeological boreholes, discontinuous regional stratigraphy, varying lithological characteristics of strata, and inadequate identification of hidden regional faults. To address these issues, various solutions have been implemented, such as analyzing major and trace elemental compositions, isotopes, groundwater temperature and level, and employing various data processing methods. Hydrochemical and multi-isotopic methods have proven to be effective tools for differentiating groundwater from different aquifers and tracing the sources of leakage waters (Duvert et al. 2015; Li et al. 2018; Qian et al. 2017; Wu et al. 2017; Zhang et al. 2020a, b).

The hydrochemical approach relies on the fact that different surface waters or groundwaters have distinct compositions, which are primarily influenced by their source of ions and the physicochemical processes they have undergone, such as water–rock interactions, evaporation, and mixing of water bodies from multiple sources (Li et al. 2018; Wu et al. 2017; Zhang et al. 2020a, b). Isotopic fractionation of hydrogen and oxygen occurs during the water cycle (evaporation, condensation, descent, infiltration, and runoff) because the thermodynamic properties of water molecules are affected by the mass of the hydrogen and oxygen atoms (Gat 1996). The hydrogen and oxygen isotopes of atmospheric precipitation are influenced by factors such as latitude, altitude, and continentality (Sun et al. 2023; Terzer-Wassmuth et al. 2021). River water exhibits similar hydrogen–oxygen isotopes to atmospheric precipitation in the region, but evaporation in arid areas leads to an enrichment of heavy isotopes in river water (Craig 1961; Han 2018; Liang et al. 2017). Groundwater can also alter the oxygen isotopes in water bodies due to prolonged water–rock interactions, particularly the dissolution of silicates and carbonates (Hao et al. 2019; Yang et al. 2020). Additionally, water isotopes can indicate the mixing of different water bodies and the hydraulic connection between them, such as in coal mining areas and karst areas (Ghosh et al. 2018; Guo et al. 2019; Qin et al. 2021; Yang et al. 2020; Zhang et al. 2023).

Boron (B), a highly soluble element, exhibits two stable isotopes (^{10}B and ^{11}B), and its isotopic compositions in nature range from − 70‰ to + 75‰ (Xiao et al. 2013). In natural samples, boron forms B–O bonds and is bound by oxygen. Due to its lack of valence change and limited involvement in redox chemistry, the fractionation of B isotopes in nature is primarily controlled by the structural ratio of the B species in the sample. This ratio is determined by the pH and the B concentration (Marschall and Foster 2018). Fractionation processes, such as evaporation, ion exchange, gas or liquid phase diffusion, and adsorption, can lead to variations in the relative enrichment of B isotopes in the different structural phases (Palmer et al. 1992; Vengosh et al. 1992; Xiao and Wang 2001).

There are some differences in the range of B isotope compositions in different geologic carriers. Marine and terrestrial water bodies, for instance, exhibit distinct B isotopic compositions. Seawater typically has δ^{11}B values around + 40‰, while subsurface freshwater generally has δ^{11}B values below + 10‰ (Xiao et al. 2013). Consequently, the intrusion of seawater into coastal areas significantly increases the B content and alters its isotopic composition in groundwater. Studies by Mahlknecht et al. (2017) and Mao et al. (2020) in the coastal zones of the southern California Peninsula, Mexico, and Jiangsu Province, China, respectively, have demonstrated that highly saline groundwater exhibits δ^{11}B values similar to those of seawater, indicating the influence of seawater intrusion on the salinization process. By applying similar principles, B isotopes can be used to trace the sources of solutes, detect groundwater contamination in urban and mining areas, determine the origins of metal and non-metal deposits, and reconstruct rock weathering processes (Fan et al. 2015; Mao et al. 2019; Zhang et al. 2021, 2022; Zheng et al. 2023).

The Dongming opencast coal mine, located in Hulun Buir, northeastern Inner Mongolia suffers groundwater leakage (Fig. 1a), which poses a threat to slope stability, production safety, and the sustainable development of valuable water resources. Previous hydrogeological investigations have identified two main aquifers: the Quaternary pore aquifer and the Cretaceous pore-fissure aquifer. Additionally, comprehensive geophysical investigations using surface nuclear magnetic resonance and transient electromagnetic methods have confirmed the presence of abundant groundwater, primarily in sediments located at depths below 100.0 m in the northern and northwestern parts of the mining area (Shan et al. 2018). Field investigations have shown that groundwater flows into the mining pits from both of these aquifers. However, the primary sources of water and the possibility of a hydraulic connection between the two aquifers remain unclear.

To address this issue, various types of water, including snow water, river water, groundwater from the different aquifers, and coal pit waters, were collected from the Dongming opencast coal mine and its surroundings. These water samples were then analyzed for their chemical compositions and H–O–B isotopes. By combining these results with previous hydrogeological investigations and published geochemical data, the main sources of the water leakage and the evolution of different water sources, as well as their controlling mechanisms, were defined. Furthermore, the hydraulic relationships between the different aquifers was established.

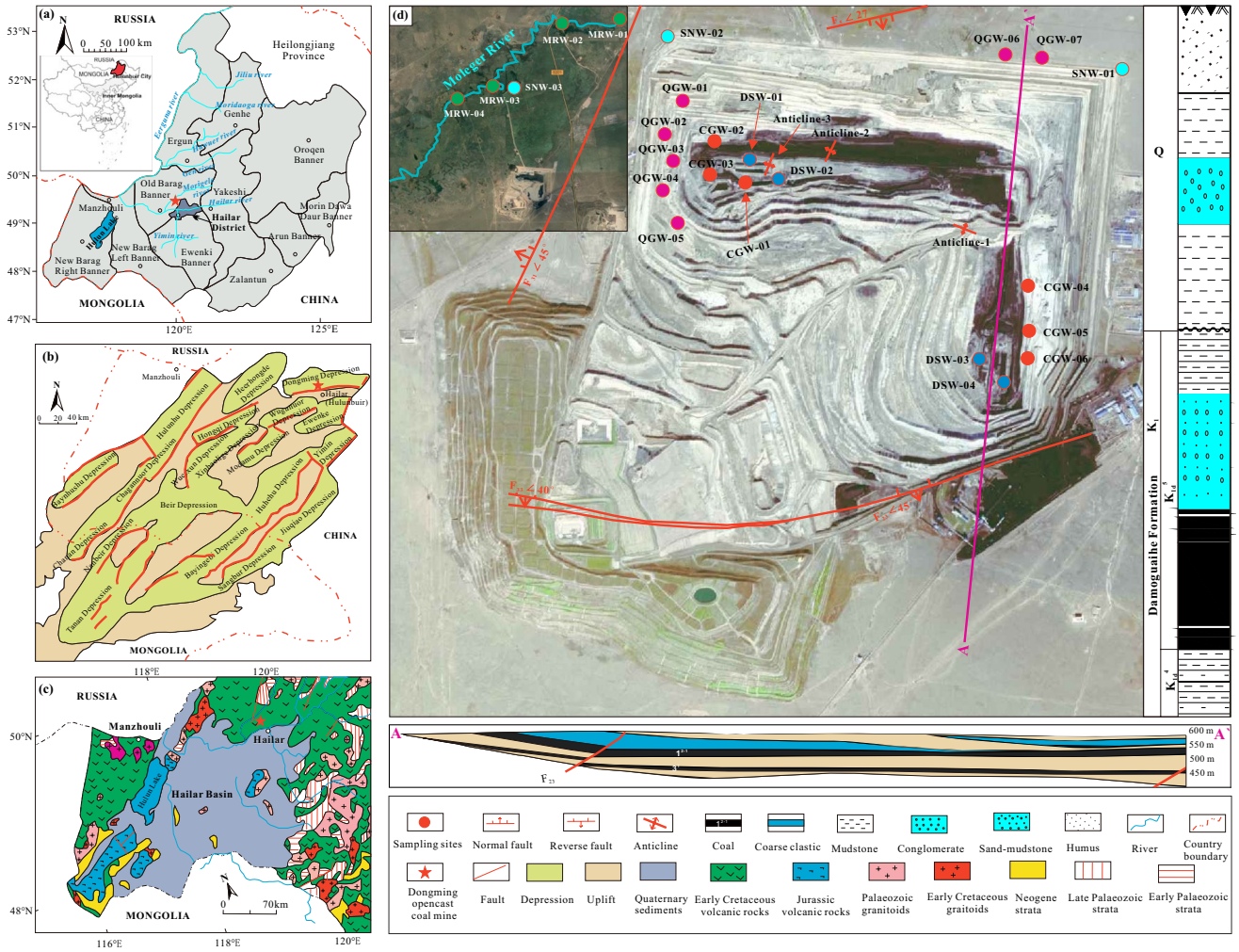

Fig. 1 **a** The location of Dongming opencast coal mine. **b** Tectonic units of the Hailar Basin. The Hailar Basin extends into Mongolia is called the Tamtsag Basin. **c** Geological sketch map of the Hailar Basin. **d** Sampling sites of different waters, drill columnar section, and stratigraphic section of the Dongming opencast coal mine (modified after IMBGMR 1991; Ji et al. 2019)

Study Area

Geographical and Geological Setting of the Study Area

The Dongming opencast coal mine is located northwest of Hailar city. It is a flat area with an altitude ranging from 605.0 to 630.0 m (Fig. 1a). The mining area is approximately 5 km from the Morigele River, which has a water level of 598.6–602.9 m. About 20 km south of the mining area, the Hailar River has an average water level of 498.3 m. The climate in this area is characterized by a mid-temperate continental monsoon climate. The temperature ranges from − 48 °C to 37.7 °C, with an average of − 2.6 °C. The maximum annual precipitation is 542.9 mm, with an average of 315.0 mm. The annual average evaporation is 1344.8 mm.

Tectonically, the opencast coal mine is situated in the Dongming depression, which is one of the sags in the Hailar Basin (Fig. 1b). The Hailar Basin is located in the eastern part of the Central Asian orogenic belt and is developed in the Paleozoic Erguna and Xing'an Blocks (Ji et al. 2019). It covers an area of 79,610 km^2 and is bounded by the Mongol-Okhotsk suture zone in the northwest and the Great Xing'an Range in the southeast. The part of the basin that extends into Mongolia is known as the Tamtsag Basin (Li et al. 2014; Wan 2006). During the middle and late Mesozoic, a series of extensional basins, including the Hailar Basin, began to develop in northeast China. These basins were rich in oil and coal resources (Jia et al. 2019). The Hailar Basin is mainly confined by NE-SW trending faults, and 16 sags were formed in this extensional environment during the late

Mesozoic to Cenozoic. Nearly 5000 m of non-marine sediments were deposited in these sags (A et al. 2013; Meng et al. 2013). According to the stratigraphic division, the area mainly includes the pre-Jurassic Budate Group, the Upper Jurassic–Lower Cretaceous Xing'anling and Zhalainuoer groups, and the Upper Cretaceous–Paleocene Beierhu Group (Wan 2006). The Budate Group is usually the basement of the late Mesozoic basins, and the Xing'anling Group includes the Tamulangou, Tongbomiao, and Nantun formations, in ascending order. The Tamulangou Formation has a small distributional range and is mainly composed of late Jurassic bimodal volcanic rocks. The Tongbomiao and Nantun formations are mainly composed of fluvial lacustrine conglomerate, sandstone, silty sand, and mudstone interbedded with a small amount of volcanic rocks. The overlying Zhalainuoer Group can be divided into the Damoguaihe and Yimin formations, in ascending order. These two formations consist mainly of fluvial lacustrine facies detritus and coal seams. The uppermost Beierhu Group includes the late Cretaceous Qingyuangang, Paleocene Huchashan formations, and Quaternary unconsolidated sediments (Ji et al. 2019; Jia et al. 2019; Wan 2006).

This study focuses on the Dongming depression, specifically the strata revealed by drilling results in the opencast coal mine. The strata mainly consist of the Quaternary (Q) strata and the coal-bearing section (K_{1d}) of the Lower Cretaceous Damoguaihe Formation. However, the Paleocene strata are missing (Fig. 1c). The Quaternary strata overlie the coal-bearing strata with a thickness ranging from 4.9 m to 78.0 m. The lithology of the strata includes brownish yellow clay, sandy clay, gravel, a small amount of medium sand, fine sand, silt, a small amount of brick red gravel, and humus. The underlying Damoguaihe Formation ($K_{1d)}$ is characterized by extra thick or medium thick coal-bearing strata. The entire coal-bearing stratum is approximately 595.0–1540.0 m thick and is in conformable contact with the underlying Nantun Formation. Based on lithology, the Damoguaihe Formation is divided into five rock sections in descending order: coal-bearing (K_{1d}^{5}), sandy mudstone (K_{1d}^{4}), middle glutenite (K_{1d}^{3}), mudstone (K_{1d}^{2}), and glutenite (K_{1d}^{1}) sections (Fig. 1d).

In the opencast mine, only the coal-bearing and sandy mudstone sections are observed. The coal-bearing section (K_{1d}) primarily consists of black brown coal, carbonaceous mudstone, gray dark gray mudstone, gray light gray siltstone, fine sandstone, medium sandstone, coarse sandstone, and sandy conglomerate. The strata in this section is relatively stable throughout the area, with a thickness ranging from 73.6 m to 178.1 m and an average thickness of 139.4 m. It is thicker in the middle of the opencast mine and gradually thins towards the margin. The coal-bearing section is composed of 14 coal strata and is characterized by two extremely thick coal seams (1^{2-1} and 3^{1}) (Fig. 1d). The main mining target is the 1^{2-1} coal seam, which has a minable thickness ranging from 8.9 m to 25.5 m and an average thickness of 17.5 m. The 3^{1} coal seam has a thickness ranging from 1.0 m to 19.1 m with an average thickness of 11.7 m. The buried depth of the 1^{2-1} coal seam ranges from 40.0 m to 120.0 m with an average depth of 74.0 m, while the 3^{1} coal seam is buried at depths ranging from 120.0 to 230.0 m, with an average depth of 150.0 m.

Hydrogeology of the Study Area

Based on the characteristics of the water-bearing medium, groundwater flow system, water yield properties, and hydrochemical characteristics of the aquifer, the aquifers in the area can be classified into two types: the Quaternary porous aquifer and the fractured porous aquifer of the Upper Damoguaihe Formation in the Lower Cretaceous. The Quaternary aquifer is widely distributed in the mining area, following the pattern of ancient river channels. It has an average thickness of 26.2 m, ranging from 0 to 56.2 m, and mainly consists of loose gravel layers with well-developed pores. The water level is typically buried at a depth of about 10.0 m, and the groundwater type is phreatic water. The overall flow direction is from northeast to southwest, influenced by hydrogeological conditions and lithologic structural characteristics. The aquifer is primarily recharged by atmospheric precipitation and lateral runoff, while discharge occurs through evaporation, water usage in industrial and domestic settings, or recharge into the lower coal-bearing strata through tectonic windows.

The fractured porous aquifer of the Upper Damoguaihe Formation is present throughout the mining area. It is primarily composed of lignite, with some coal seams containing middle sandstone, coarse sandstone, and conglomerate in the roof. The aquifer has a thickness ranging from 10.0 to 60.0 m, and the water yield of individual wells is less than 500 m^3 per day. The top and bottom of the aquifer are typically composed of mudstone, siltstone, or fine sandstone, providing good water insulation. The bottom plate has a thickness ranging from 2.0 to 21.0 m, while the top plate has a thickness ranging from 2.0 to 16.0 m. However, due to structural influences, local uplift, and roof denudation, permeable "skylights" exist, allowing runoff recharge to the Quaternary aquifer. The main recharge sources for the fractured porous aquifer are lateral runoff recharge and recharge from the Quaternary aquifer at the "skylight" locations.

Materials and Methods

In this study, a total of 24 water samples were collected: three snow water (SNW) samples, four Morigele River water samples (MRW), seven groundwater samples from Quaternary strata (QGW), six groundwater samples from coal strata (CGW), and four water samples from the drainage sump (DSW) of the mining area (Fig. 1c). The SNW samples were collected from the northern region of the mine, near the Morigele River. The QGW samples were obtained from leakage through the mine edge and shallow wells. The CGW samples were primarily collected from coal seam leakage in the mine pit. The DSW samples were collected from the drain pit in the mining area, which contained a mixture of water from the Quaternary strata and coal seam seepage. All samples were collected in mid-August 2020, except for the SNW samples, which were collected in April 2020 because the study area experiences cold temperatures and frequent snowfall in April, while August is a period of increased rainfall. Each sample was collected in acid-washed 500 mL low-density polyethylene (LDPE) bottles, which were rinsed three times with the sampled water. Within 48 h of collection, each sample was filtered using a 0.45 µm Luerloch syringe filter with a polypropylene membrane, and transferred into acid-washed 125 mL LDPE bottles.

The K^+, Na^+, Ca^{2+}, Mg^{2+}, $SO_4{}^{2-}$, and B^{3+} cations were measured by inductively coupled plasma optical emission spectrometry (ICP-OES, ICAP6500 DUO, Thermo Fisher Scientific, US) with an analytical precision exceeding ± 5%. $HCO_3{}^-$ and Cl^- were measured by volumetrically and ion chromatography (ICS-5000A), with a test accuracy of < 0.3%. All testing work was conducted at the Qinghai Institute of Salt Lakes, Chinese Academy of Sciences.

Hydrogen and oxygen isotope determination was completed by online analysis of element analyzer flashEA 1112 HT and mass spectrometry MAT 253 (Zhang et al. 2011) at the Wuhan Institute of Geology and Mineral Resources. International standards V-SMOW, GISP, GBW04459, and duplicate samples (the number of standard and duplicate samples is 30% of the total number of samples) were used to monitor quality in the analysis process; Measured $\delta D_{v\text{-}smow}$ and $\delta^{18}O_{v\text{-}smow}$ values of V-SMOW were 0.60 ± 0.22 ‰ and 0.07 ± 0.12 ‰, $\delta D_{v\text{-}smow}$ and $\delta^{18}O_{v\text{-}smow}$ values of GISP were − 189.30 ± 1.20 ‰ and − 24.75 ± 0.12 ‰, and $\delta D_{v\text{-}smow}$ and $\delta\ ^{18}O_{v\text{-}smow}$ values of GBW04459 were − 63.20 ± 0.90 ‰ and − 8.59 ± 0.05 ‰ respectively. These data and the repeated determination results are consistent with their recommended values within the error range, indicating that the determination results are reliable.

The $^{11}B/^{10}B$ ratios of samples were determined by positive thermal ionization mass spectrometry (Triton, Thermo Fisher Finnigan, Germany) at the Qinghai Institute of Salt Lakes, Chinese Academy of Sciences. The detailed sample preparation and analysis steps are described by He et al. (2013). The boron isotopic compositions of samples were expressed as $\delta^{11}B = [(^{11}B/^{10}B)_{sample}/(^{11}B/^{10}B)_{standard}] - 1$, where the standard is NIST SRM 951 (supplemental Table S-1). The $^{11}B/^{10}B$ ratio of NIST SRM 951 was determined repeatedly to be 4.05537 ± 0.00004 (2σ, $n = 4$).

Results

Hydrochemistry of the Different Waters

The analytical results are shown in supplemental Table S-1. The pH values of the different waters are distinct. The pH values of CGW, DSW, QGW, and MRW in the mining area were alkaline, with a range from 7.3 to 8.9, while the pH values of the SNW were circumneutral (7.4–7.7). The average TDS was 1021.49 mg/L for CGW, 1120.53 mg/L for DSW, 685.95 mg/L for QGW, 407.09 mg/L for MRW, and 9.07 mg/L for SNW.

The major ion compositions of the different waters are plotted in the Piper diagram (Fig. 2). Na and HCO_3 are the dominant cation and anion in all of the waters, which is in accordance with the chemical weathering background of the region (Zheng and Lv 1994). The hydrochemistry of the QGW and MRW are comparable, and in the cationic diagram, Na + K proportions of those samples generally exceed 40%, Mg and Ca proportions are less than 40%, while in the anionic graph, HCO_3 are dominant, accounting for about 80% of the total anions, and SO_4 and Cl are generally lower than 20% and 10%, respectively. In the diamond diagram, most of the QGW and MRW samples are located in the Ca–HCO_3 region, indicating that the QGW and MRW have a similar origin or close hydraulic connection.

The hydrochemistry of the CGW samples was relatively dispersed, belonging to the Ca–Na–HCO_3 or Na–HCO_3 types, with Na + K and HCO_3 proportions ranging from 60%–80%, respectively; the Mg, Ca, Cl, SO_4 proportions were generally < 20%, suggesting that the waters from the coal-bearing strata have different origins or evolution processes. All of the DSW samples had similar major ion compositions, and are Ca-Na-HCO_3 type, with Na + K, HCO_3 proportions higher than 60%, and Mg, Ca, Cl, SO_4 generally < 20%. Hydrochemistry of the DSW samples is different from other waters in the study area, and presents a mixing origin of the QGW and CGW.

In addition, the hydrochemistry of the SNW samples is similar to the CGW and DSW, with high Na and K, and low Mg and Ca concentrations, indicating that local meteoric waters are probably influenced by open pit coal mines near the study area. The DSW had the highest trace element B^{3+} content, with an average value of 0.23 mg/L, followed by

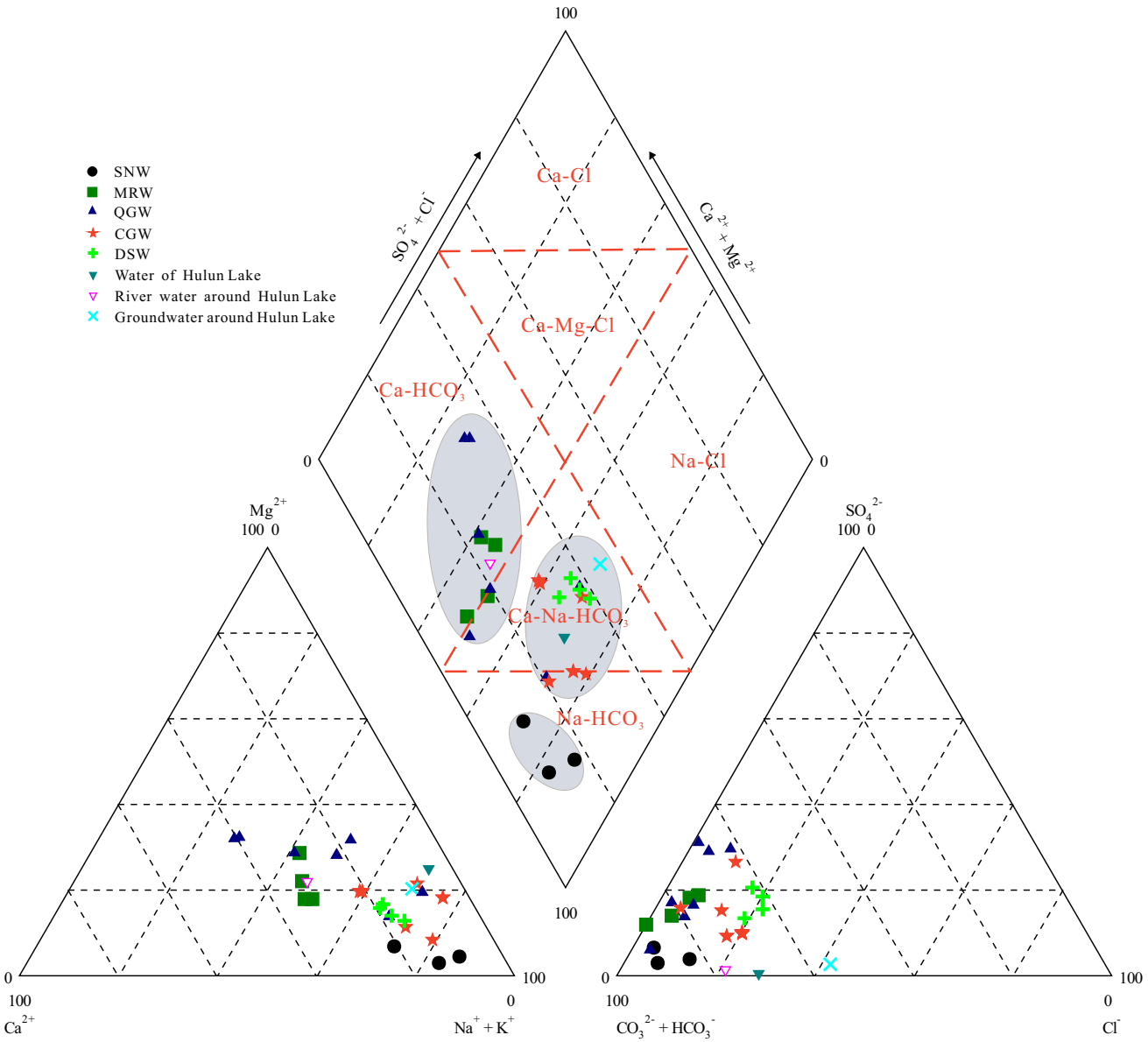

Fig. 2 The piper diagram of different waters in the study area. SNW (snow water), MRW (Morigele River water), QGW (groundwater from the Quaternary strata), CGW (groundwater from coal strata), DSW (water in drainage sump). The ion compositions of Hulun Lake water, river water and groundwater around Hulun Lake are from Han (2018)

CGW with average value of 0.18 mg/L, and the QGW with average value of 0.10 mg/L.

H–O-B Isotopes

The SNW samples had the most negative hydrogen and oxygen isotopic compositions; the average δD and $\delta^{18}O$ were − 146.96‰ and − 18.17‰, respectively. The H–O isotopic compositions of the other waters were similar. The average δD and $\delta^{18}O$ of CGW were − 105.67‰ and − 13.21‰, and those of DSW were − 104.79‰ and − 12.87‰. The QGW has the highest δD and $\delta^{18}O$ values of − 103.82‰ and − 12.28‰.

The B isotopic compositions of the CGW samples ranged from 10.74‰ to 31.58‰ with a mean of 21.71‰, while those of the DSW ranged from 20.18‰ to 29.02‰, with a mean of 25.16‰. The river waters and Quaternary groundwaters generally had low B isotopes, ranging from 1.68‰ to 18.30‰ with an average value of 7.77‰ for QGW, and from 4.05‰ to 8.48‰, averaging 6.27‰ for MRW.

Discussion

The Mechanism of Salinization and Ion Sources of the Different Waters

The determination of ion sources and their evolution is crucial for understanding the formation of different types of water. The Gibbs diagram provides a visual representation of the natural factors (such as evaporation concentration, rock weathering, and precipitation control) that influence the major ion compositions of surface water in a specific area (Gibbs 1970). The distribution pattern of major ion compositions of MRW and DSW suggests different salinization mechanisms for these waters (Fig. 3a). The TDS of DSW exceeded those of MRW, and the Na/(Na + Ca) weight ratios ranged from 0.7 to 0.9, which is close to the transitional line between rock weathering and evaporation. This indicates that the enrichment of ions in DSW is primarily controlled by weak rock weathering and evaporation (Fig. 3a). However, the Cl/(Cl + HCO_3) weight ratios of DSW ranged from 0 to 0.2, which is outside the range expected for evaporation and rock weathering. This abnormal enrichment of HCO_3 compared to Cl is consistent with the high HCO_3 hydrochemical background of surface water in the study area, which includes freshwater lakes and carbonate-type salt lakes (Zheng and Lv 1995). The water from Hulun Lake, which is influenced by evaporation, also exhibits low Cl/(Cl + HCO_3) weight ratios (Fig. 3b). The enrichment of HCO_3 may be attributed to the dissolution of carbonates and weathering of silicates (Appelo and Postma 2005), which are widely distributed in the study area (IMARBGMR 1996; Zheng and Lv 1994, 1995). On the other hand, the MRW had relatively low TDS and Na/(Na + Ca) weight ratios compared to DSW, as well as extremely low Cl/(Cl + HCO_3) weight ratios, indicating that rock weathering is the dominant source of solutes. This is consistent with the ion sources of most rivers worldwide (Gaillardet et al. 1999; Hu et al. 2023). The SNW are typical precipitation waters and are located in the lower right corner of the Na/(Na + Ca) vs. TDS diagram. However, the SNW also exhibit low Cl/(Cl + HCO_3) weight ratios, indicating the strong influence of the local geochemical background on precipitation.

The Ca/Na ratios in detrital strata, particularly in arid regions, can be altered by the leaching of Na salts. This can complicate the interpretation of the Gibbs diagram and mask the influence of evaporation (Marandi and Shand 2018). However, the conservative element of Mg, primarily derived from rock weathering, increases in conjunction with evaporation (Bąbel and Schreiber 2014). Consequently, the Mg/Na and Mg/Ca ratios can serve as indicators of the leaching of salt-bearing strata and evaporation, respectively. In Fig. 3c, most of the CGW, DSW, and SNW samples are located in the bottom left quadrant, indicating relatively weak evaporation and weathering of Mg-rich rock. However, the solute sources are mostly influenced by the leaching of Na and Ca salts. A few samples of CGW and QGW in the upper left quadrant exhibit high ratios of Mg/Ca and low ratios of Mg/Na, suggesting a potential weak evaporation process for these waters (Liang et al. 2017). During the evaporation process, Na and Cl concentrations will increase, while Mg and Ca concentrations will decrease due to carbonate precipitation. Some of the MRW and QGW samples are primarily influenced by weathering of Na-rich rocks.

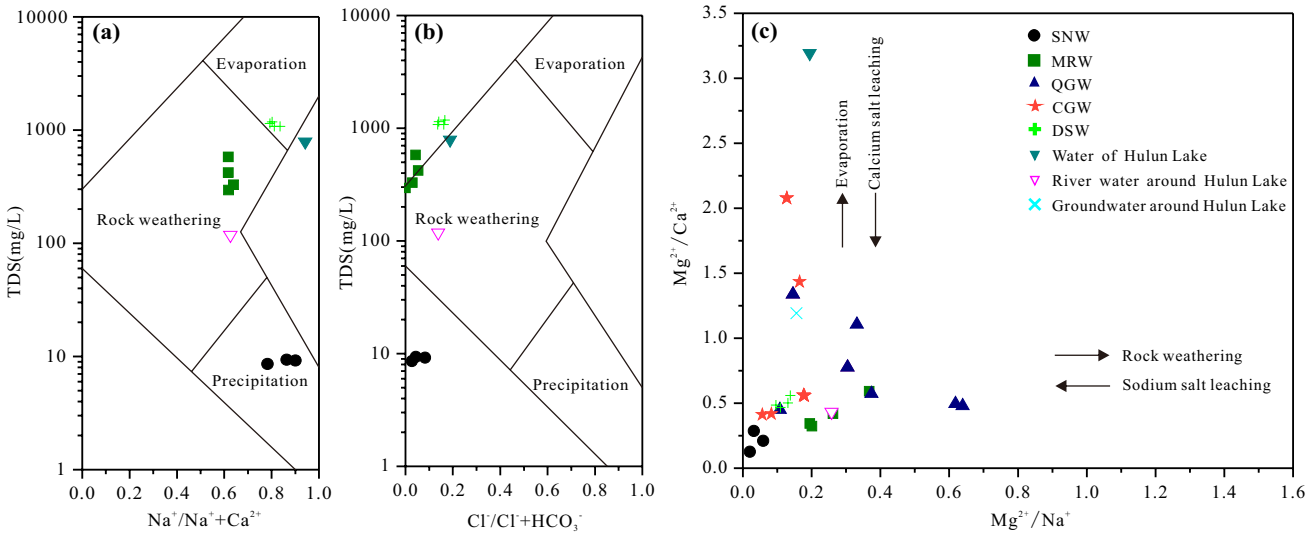

Fig. 3 **a**, **b**, Variation of the weight ratio Na/(Na + Ca), and Cl/(Cl + HCO_3) vs. TDS of different surface waters; **c**, the weight ratio of Mg/Ca vs. Mg/Na of different waters in the study area

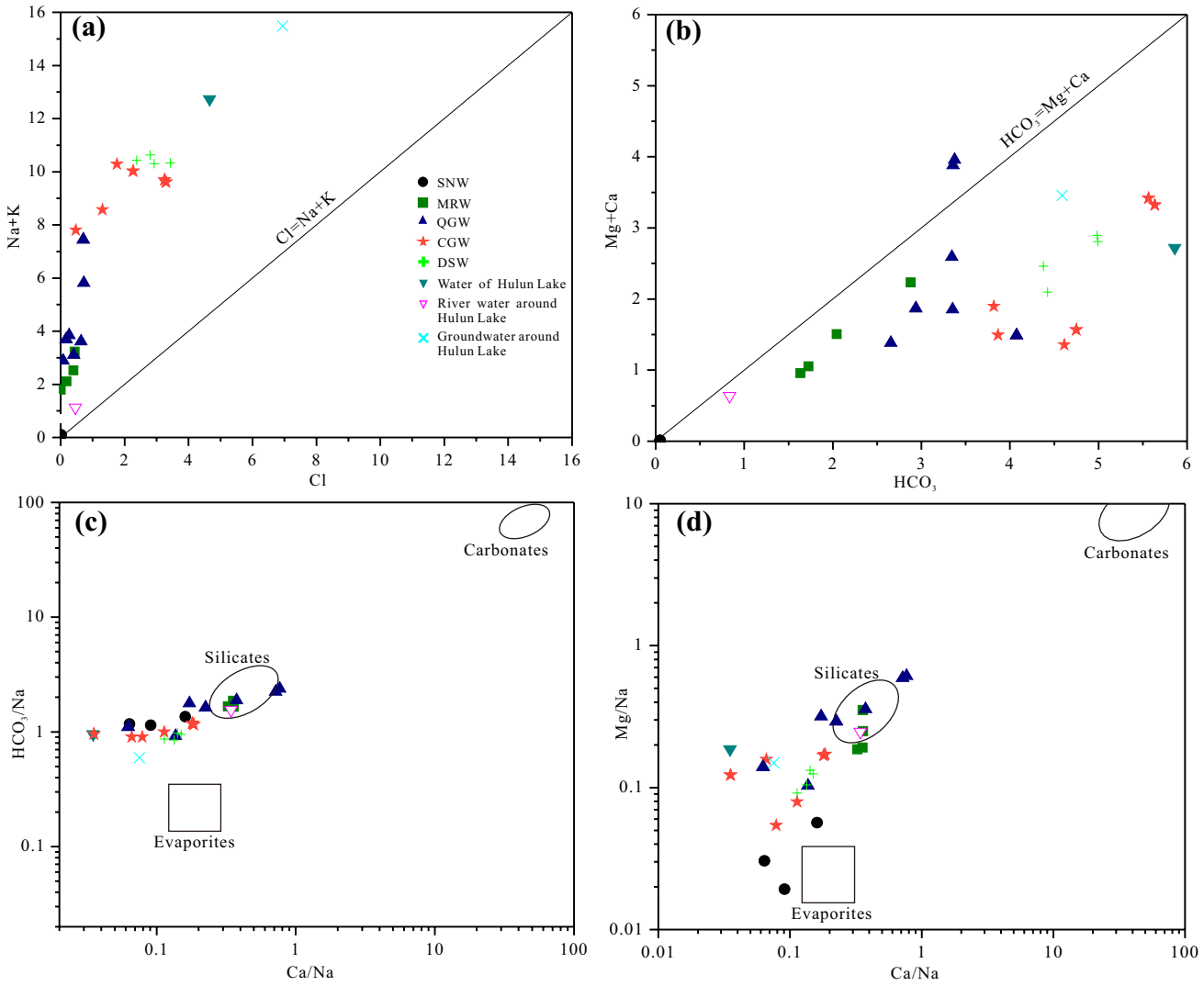

Fig. 4 Mixing diagrams of ion molar ratios of different waters. **a** Na + K vs. Cl molar ratio, **b** Mg + Ca vs. HCO_3 molar ratio, **c** and **d** Na-normalized molar ratios of HCO_3, Ca, and Mg, Ca

In general, the production of Na and K is primarily attributed to the weathering of silicates and evaporites. When the chemical compositions of waters are influenced by the dissolution of chloride salts, the molar ratio of (Na + K)/Cl tends to be close to 1. However, in this study, Fig. 4a shows that most of the water samples deviate from the Na + K = Cl line and are located towards the higher Na + K end member. This suggests that in addition to the dissolution of minor chloride salts, silicate weathering may contribute significantly to the abundance of Na and K in the CGW, QGW, DSW, and MRW. The higher Na + K values, along with higher Cl concentrations in CGW and DSW compared to QGW and MRW, indicate that CGW and DSW have undergone slight concentration through evaporation.

To investigate the influence of carbonate dissolution on the waters' chemical compositions, the molar equivalents of Mg and Ca are plotted against HCO_3 (Fig. 4b). Most of the waters in this study are located to the right of the carbonate dissolution line. This suggests that excess HCO_3 ions were provided through the dissolution of Na_2CO_3 salts or the weathering of Na-silicates (Yang et al. 2020; Zhao et al. 2022; Zheng and Lv 1994, 1995). Considering that Mg, Ca, and Na in natural waters primarily originate from the weathering of silicates and carbonates (Fu et al. 2018; Silva and Lima 2023), the presence of excess Na and HCO_3 ions in CGW, DSW, and QGW (Fig. 4a) indicates the dissolution of Na_2CO_3 salts or the weathering of Na-silicates in the coal-bearing and Quaternary strata. During this process, the reaction between silicates and $CO_2 + H_2O$ releases alkali cations (Mg, Ca, K, and Na) and forms HCO_3 and H_2SiO_3 (Guo et al. 2023; Liu et al. 2020). The existence of clay minerals resulting from the weathering of plagioclase

(albite and K-feldspar) further supports this phenomenon (Gaillardet et al. 1999).

Furthermore, the molar ratios of Mg/Na, Ca/Na, HCO_3/Na of the dominant controlling factors (silicates weathering, carbonates dissolution, and evaporites dissolution) of natural waters are constrained, based on the chemical composition analysis of 60 large rivers around the world (Gaillardet et al. 1999). Based on these ratios, the composition of CGW and DSW falls between the end members of silicates weathering and evaporite dissolution, with a closer proximity to silicates weathering (Fig. 4c and d). Additionally, most of the samples from the QGW and MRW are within the range of silicates weathering. The presence of excess Na from silicates weathering leads to lower ratios of HCO_3/Na and Mg/Na in CGW and DSW than in QGW and MRW. These observations suggest that carbonate dissolution weakly influence the composition of these waters, as they deviate significantly from the end member associated with this factor.

Origin of the Different Waters: H–O Isotopes

H–O isotopes serve as valuable tracers for identifying the sources, connections, and circulation processes of water bodies. The global meteoric water line (GMWL, $\delta D = 8\ \delta^{18}O + 10$) is generally used to analyze the characteristics of the H–O isotopic compositions in different regions (Craig 1961; Guerra et al. 2023; Hughes and Crawford 2012). The local meteoric water line (LMWL, $\delta D = 6.68\ \delta^{18}O\text{-}5.98$, $R^2 = 0.9$) was derived from the weighted average of hydrogen and oxygen isotopes in rainwater and snowmelt near Xinbaerhu Right Banner, south of Hulun Lake, in June 2016 (Han 2018). Additionally, the local evaporation trend line (ETL, $\delta D = 4.99\ \delta^{18}O\text{-}32.89$, $R^2 = 0.89$) was established based on Han (2018).

The snow waters collected in this study, referred to as SNW, exhibit the lowest $\delta D\text{-}\delta^{18}O$ values of the water samples, but still excced those of the snow waters from Hulun Lake, suggesting the occurrence of evaporation processes in the SNW (Han 2018). The deviation of the SNW from the LMWL can be attributed to weak evaporation. The H–O isotopic compositions of CGW, QGW, DSW, and MRW are similar and cluster in the bottom right of the LMWL, which aligns with the arid climate in the study area. This implies a close relationship between these different water bodies. It is likely that the CGW and QGW originate from MRW. The H–O isotopes of these waters slightly exceed those of the intersection point of the LMWL and ETL, and some of the MRW and QGW fall on the ETL, indicating that the river and underground waters in this study have undergone evaporation. However, the relatively lower H–O isotopes of these waters, compared to the Hulun Lake water, suggest a weak evaporation process. Most of the underground waters exhibit

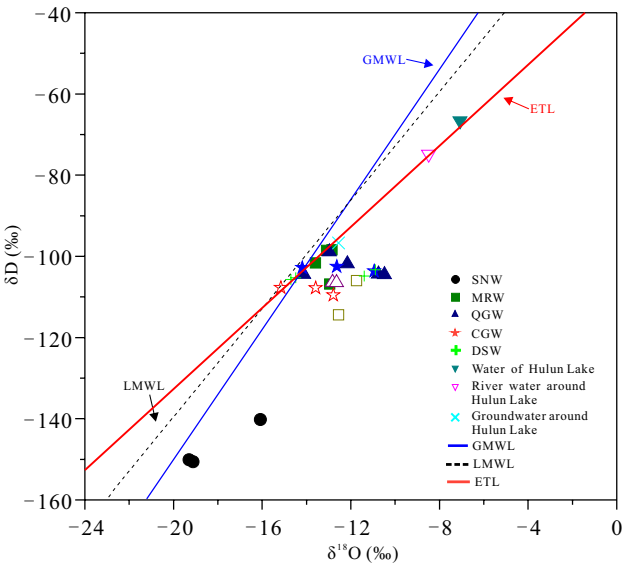

Fig. 5 H–O isotopic compositions of differen waters in study area. *GMWL* global meteoric water line (modified from Craig 1961); *LMWL* local meteoric water line (modified from Han 2018); *ETL* evaporation trend line (modified from Han 2018)

a slight positive shift in O isotopes, indicating water–rock interactions during burial and flow processes (Fig. 5).

Thus, the MRW, QGW, CGW, and DSW exhibit similar H–O isotopes, indicating a close hydraulic connection between the river and underground waters. Despite being from different aquifers, the CGW and QGW share the same water origin and are related to the river waters in the study area.

Hydraulic Connection Between the Different Aquifers: Insights from the B Isotopes

The preceding discussion demonstrates that regional waters, including CGW and QGW from various aquifers, can exhibit similar origins and similar hydrochemical evolution processes. Assessing the hydraulic connectivity between different aquifers proves challenging. Additionally, distinguishing the primary water sources in coal mine pits through hydrochemical and H–O isotope analysis poses difficulties (Yang et al. 2020; Zhao et al. 2022). Similar challenges have been encountered in other coal mines, particularly underground mines. In this study, the B isotopes of different waters exhibited major variations and were distributed among the different end members in the $\delta^{11}B$ vs. 1/B diagram. This suggests the potential for effectively evaluating the hydraulic connectivity of different aquifers and rapidly identifying the main sources of water in coal mines.

The MRW exhibited the lowest concentrations and isotopic compositions of B, while the QGW samples showed increasing B concentrations and isotopes (Fig. 6). Interestingly, one of the QGW samples had similar B concentrations and isotopes to those of the MRW, indicating a

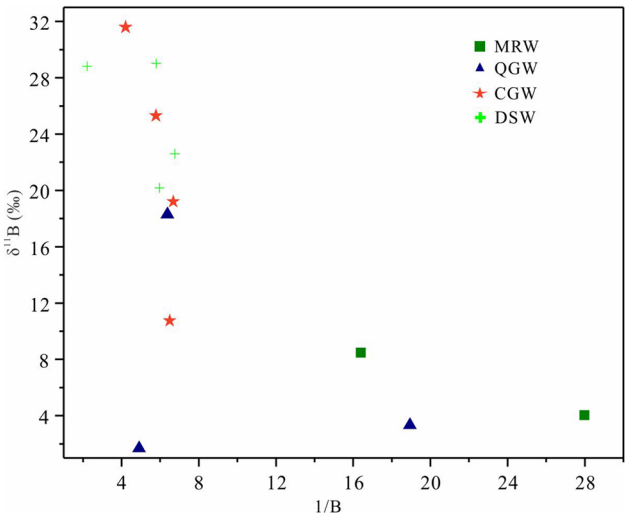

Fig. 6 Plots of $\delta^{11}B$ vs. 1/B of different waters in the study area

close recharge connection between the QGW and river waters. The higher B concentrations and isotopes in the other QGW waters may be attributed to the relatively poor hydraulic connectivity between the Quaternary strata and the rivers at the sampling sites. Various factors can lead to changes in B isotopes in natural waters, such as intense evaporation accompanied by mineral precipitation, rock weathering, and clay adsorption (Lemarchand et al. 2007; Mao et al. 2019; Marschall and Foster 2018; Ruhl et al. 2014). In this study, the extremely low TDS of the waters exclude the possibility of evaporation and mineral precipitation, suggesting that rock weathering is the dominant solute source. However, negative or lower B isotopic compositions can be produced by the weathering of silicates and coal, as these materials generally have lower B isotopes. For instance, tourmaline in magmatic rock has isotopic compositions ranging from − 2‰ to − 30‰, biotite has an isotopic composition of − 20.1‰, plagioclase ranges from − 13.5‰ to − 10.4‰, quartz has an isotopic composition of − 9.9‰, and coals have isotopic compositions ranging from − 70‰ to − 1.1‰ (Williams and Hervig 2004; Xiao et al. 2013; Zhao et al. 2015). Therefore, the elevated B isotopes in the waters are likely related to clay adsorption, which can result in B isotopic fractionation of up to 15‰ to 20‰, and an increase in dissolved B isotopes (Ercolani et al. 2019; Mao et al. 2019). The poor hydraulic connectivity between the aquifers and the river waters, which indicates a long duration of underground water flow, coupled with a strong clay adsorption process, contributes to the elevated B isotopes in the waters. The CGW samples had the highest B concentrations and isotopes, and there was significant variation in B isotopes among the different CGW waters, suggesting poor hydraulic connectivity between the coal-bearing strata and the river waters. Furthermore, even within the same aquifer, there was a large discrepancy in B isotopes, indicating differences in hydraulic connectivity between the different sampling sites and the river water. Therefore, B isotopes serve as sensitive tracers for evaluating hydraulic connectivity in the study area.

The B isotopes of the DSW are situated between those of the CGW and QGW and are close to the CGW. This is consistent with the DSW being a mixture of the CGW and QGW. The hydrochemistry and B isotopes of the DSW and CGW are similar, indicating that the DSW primarily originates from the CGW. Although the QGW is closely connected to the river water, the coal mine has implemented measures to prevent the shallow QGW from leaking into the mine pit. Currently, the water leakage in the mine pit mainly comes from the coal-bearing aquifer. In the future, B isotopes should be analyzed in additional samples to identify the leakage sites that have the strongest hydraulic connectivity with the river water. This will enable more effective prevention of water leakage into the mine pit.

Conclusions

In order to study the origin of groundwater in the Dongming opencast coal mine, different waters including river water, groundwater in Quaternary strata and coal-bearing strata, snow water, drainage sump water were sampled. Hydrochemical and H–O–B isotopic compositions of the waters were analyzed, and the following conclusions were reached.

(1) The hydrochemical type of groundwater in the coal-bearing strata and drainage sump water is Ca–Na–HCO_3, the Morigele River water and the groundwater in the Quaternary strata are Ca-HCO_3, and the snow water is Na–HCO_3. Na and HCO_3 are dominant ions in all of the water samples, which is in accord with the geochemical setting of the study area.

(2) The ratios of various ions (Mg/Ca, Mg/Na, Ca/Na, Na + K/Cl, Mg + Ca/HCO_3, and HCO_3/Na), and the Gibbs diagram of the sampled waters indicate that the weathering of rock, particularly Na-rich silicates, is the primary factor influencing the hydrochemical compositions of the groundwater.

(3) H–O isotopes suggest that all of the groundwaters are derived from river water. Additionally, the similar B isotopic compositions of the QGW and MRW demonstrate close hydraulic connection between the Morigele River and groundwater in Quaternary strata. On the other hand, the elevated B concentrations and isotopes of CGW imply a weak hydraulic connectivity between the coal-bearing aquifer and the river water.

Supplementary Information The online version contains supplementary material available at https://doi.org/10.1007/s10230-023-00963-1.

Acknowledgements The anonymous reviewers are thanked for their detailed and helpful reviews that significantly improved the manuscript. This research was financially supported by the National Key R&D Program of China (2021YFC2902004), the lnner Mongolia Science and Technology Major Special Proiect (2020ZD0020-4), and the China National Natural Science Foundation (42072284).

Funding This article is funded by The National Key R&D Program of China, 2021YFC2902004, Yifan Zeng, the lnner Mongolia Science and Technology Major Special Proiect (2020ZD0020-4), Yifan Zeng, The China National Natural Science Foundation, 42072284, Yifan Zeng.

References

A MN, Zhang FQ, Yang SF, Chen HL, Batt GE, Sun MD, Meng QA, Zhu DF, Cao RC, Li JS (2013) Early cretaceous provenance change in the southern Hailar Basin, northeastern China and its implication for basin evolution. Cretaceous Res 40:21–42. https://doi.org/10.1016/j.cretres.2012.05.005

Appelo CAJ, Postma D (2005) Geochemistry, groundwater and pollution, 2nd edn. A. A. Balkema, Leiden

Bąbel M, Schreiber BC (2014) Geochemistry of evaporates and evolution of seawater. In: Turekian KK, Holland HD (eds) Treatise on geochemistry, 2nd edn. Elsevier, Amsterdam, pp 483–548

Craig H (1961) Isotopic variations in meteoric waters. Science 133:1702–1703. https://doi.org/10.1126/science.133.3465.1702

Duvert C, Raiber M, Owen DDR, Cendón DI, Batiot-Guilhe C, Cox ME (2015) Hydrochemical processes in a shallow coal seam gas aquifer and its overlying stream-alluvial system: implications for recharge and inter-aquifer connectivity. Appl Geochem 61:146–159. https://doi.org/10.1016/j.apgeochem.2015.05.021

Ercolani C, Lemarchand D, Dosseto A (2019) Insights on catchment-wide weathering regimes from boron isotopes in riverine material. Geochim Cosmochim Ac 261:35–55. https://doi.org/10.1016/j.gca.2019.07.002

Fan QS, Ma YQ, Cheng HD, Wei HC, Yuan Q, Qin ZJ, Shan FS (2015) Boron occurrence in halite and boron isotope geochemistry of halite in the Qarhan Salt Lake, western China. Sediment Geol 322:34–42. https://doi.org/10.1016/j.sedgeo.2015.03.012

Fu CC, Li XQ, Ma JF, Liu LX, Gao M, Bai ZX (2018) A hydrochemistry and multi-isotope study of groundwater origin and hydrochemical evolution in the middle reaches of the Kuye River basin. Appl Geochem 98:82–93. https://doi.org/10.1016/j.apgeochem.2018.08.030

Gaillardet J, Dupre B, Louvat P, Allegre CJ (1999) Global silicate weathering and CO_2 consumption rates deduced from the chemistry of large rivers. Chem Geol 159:3–30. https://doi.org/10.1016/S0009-2541(99)00031-5

Gat JR (1996) Oxygen and hydrogen isotopes in the hydrologic cycle. Annu Rev Earth Planet Sci 24:225–262. https://doi.org/10.1146/annurev.earth.24.1.225

Ghosh S, Golding SD, Varma AK, Baublys KA (2018) Stable isotopic composition of coal bed gas and associated formation water samples from Raniganj Basin, west Bengal, India. Int J Coal Geol 191:1–6. https://doi.org/10.1016/j.coal.2018.02.019

Gibbs RJ (1970) Mechanisms controlling world water chemistry. Science 170:1088–1090. https://doi.org/10.1126/science.170.3962.1088

Gu DZ, Li JF, Cao ZG, Wu BY, Jiang BB, Yang Y, Yang J, Chen YP (2021) Technology and engineering development strategy of water protection and utilization of coal mine in China. J China Coal Soc 46(10):3079–3089 **(in Chinese)**

Guerra JC, Regalado CM, Ritter X, León-González M (2023) Stable isotopic composition of fog and rainfall in a Macaronesian cloud forest. J Hydrol 622:129763. https://doi.org/10.1016/j.jhydrol.2023.129763

Guo QL, Yang YS, Han YY, Li JL, Wang XY (2019) Assessment of surface-groundwater interactions using hydrochemical and isotopic techniques in a coalmine watershed. NW China Environ Earth Sci 78:91. https://doi.org/10.1007/s12665-019-8053-2

Guo YG, Zhang SX, Wang S, Zhang YW, Du J, Liao L (2023) Using stable isotope (δ2H and δ18O) and hydrochemistry to understand the genesis and hydrochemical processes of groundwater in Chongming Island, Yangtze Estuary. Environ Sci Pollut. https://doi.org/10.1007/s11356-023-28401-3

Han ZM (2018) Study on hydrogen and oxygen isotope and hydrochemistry characteristic of Hulun Lake Basin. MSc Diss, Inner Mongolia Agricultural Univ (in Chinese)

Hao CH, Huang Y, He PY, Sun W (2019) Isotope drift characteristics in Ordovician limestone karst water caused by coal mining in northern China. Mine Water Environ 38:507–516. https://doi.org/10.1007/s10230-019-00606-4

He MY, Xiao YK, Jin ZD, Ma YQ, Xiao J, Zhang YL, Luo CG, Zhang F (2013) Accurate and precise determination of boron isotopic ratios at low concentration by positive thermal ionization mass spectrometry using static multicollection of $Cs_2BO_2^+$ ions. Anal Chem 85:6248–6253. https://doi.org/10.1021/ac400066r

Hu HY, Wei RF, Zerizghi T, Du CJ, Zhao CQ, Wang ZT, Zhang J, Tan QY, Guo QJ (2023) Control mechanism of water chemistry based on long-term analyses of the Yangtze River. Sci Total Environ 892:164713. https://doi.org/10.1016/j.scitotenv.2023.164713

Huang XM, Zhang Y, Wang MX, Teng QS, Li GZ (2022) Key technical progress of water cutoff curtain technology in open-pit coal mines in China. Coal Geol Explor 50(7):1–9 **(in Chinese)**

Hughes CE, Crawford J (2012) A new precipitation weighted method for determining the meteoric water line for hydrological applications demonstrated using Australian and global GNIP data. J Hydrol 464–465:344–351. https://doi.org/10.1016/j.jhydrol.2012.07.029

Inner Mongolia Autonomous Regional Bureau of Geology and Mineral Resources (1996) Lithologic stratigraphy of inner mongolia autonomous region. University of Geosciencs Press, Beijing (in Chinese)

Ji Z, Meng QA, Wan CB, Zhu DF, Ge WC, Zhang YL, Yang H, Dong Y, Jing Y (2019) Generation of late Mesozoic felsic volcanic rocks in the Hailar Basin, northeastern China in response to overprinting of multiple tectonic regimes. Sci Rep 9:15854. https://doi.org/10.1038/s41598-019-52181-x

Jia R, Liu B, Fu XF, Gong L, Liu ZD (2019) Transformaiton mechanism of a fault and its associated microstructures in low-porosity rocks: a case study of the Tanan depression in the Hailar-Tamtsag Basin. J Mar Sci Eng 7:286. https://doi.org/10.3390/jmse7090286

Lemarchand E, Schott J, Gaillardet J (2007) How surface complexes impact boron isotope fractionation: evidence from Fe and Mn oxides sorption experiments. Earth Planet Sci Lett 260:277–296. https://doi.org/10.1016/j.epsl.2007.05.039

Li PY, Wu JH, Tian R, He S, He XD, Xue CY, Zhang K (2018) Geochemistry, hydraulic connectivity and quality appraisal of multiayered groundwater in the Hongdunzi coal mine, northwest China. Mine Water Environ 37:222–237. https://doi.org/10.1007/s10230-017-0507-8

Li SQ, Hegner E, Yang YZ, Wu JD, Chen FK (2014) Age constraints on late Mesozoic lithospheric extension and origin of bimodal volcanic rocks from the Hailar basin, NE China. Lithos 190–191:204–219. https://doi.org/10.1016/j.lithos.2013.12.009

Liang LE, Li CY, Shi XH, Sun B, Wang JJ, Zhou J (2017) Characteristics of hydrogen and oxygen isotopes of surface and ground water and the analysis of source of lake water in Hulun Lake Basin. Inner Mongolia Wetl Sci 15(3):387–390 **(in Chinese)**

Liu F, Zhao ZP, Yang LH, Ma YX, Xu YC, Gong L, Liu HY (2020) Geochemical characterization of shallow groundwater using multivariate statistical analysis and geochemical modeling in an irrigated region along the upper Yellow River, northwestern China. J Geochem Explor 215:106565. https://doi.org/10.1016/j.gexplo.2020.106565

Mahlknecht J, Merchán D, Rosner M, Meixner A, Ledesma-Ruiz R (2017) Assessing seawater intrusion in an arid coastal aquifer under high anthropogenic influence using major constituents, Sr and B isotopes in groundwater. Sci Total Environ 587–588:282–295. https://doi.org/10.1016/j.scitotenv.2017.02.137

Mao CP, Tan HB, Song YX, Rao WB (2020) Evolution of groundwater chemistry in coastal aquifers of the Jiangsu, east China: insights from a multi-isotope (δ^2H, δ^{18}O, ^{87}Sr/^{86}Sr, and δ^{11}B) approach. J Contam Hydrol 235:103730. https://doi.org/10.1016/j.jconhyd.2020.103730

Mao HR, Liu CQ, Zhao ZD (2019) Source and evolution of dissolved boron in rivers: insights from boron isotope signatures of end-members and model of boron isotopes during weathering processes. Earth-Sci Rev 190:439–459. https://doi.org/10.1016/j.earscirev.2019.01.016

Marandi A, Shand P (2018) Groundwater chemistry and the Gibbs diagram. Appl Geochem 97:209–212. https://doi.org/10.1016/j.apgeochem.2018.07.009

Marschall H, Foster G (2018) Boron isotopes the fifth element. Springer Nature, Switzerland

Meng QA, Wan CB, Zhu DF, Zhang YL, Ge WC, Wu FY (2013) Age assignment and geological significance of the "Budate Group" in the Hailar Basin. Sci China Earth Sci 56:970–979. https://doi.org/10.1007/s11430-013-4614-5

Palmer MR, London D, Morgan VIGB, Babb HA (1992) Experimental determination of fractionation of ^{11}B/^{10}B between tourmaline and aqueous vapor: a temperature-and pressure-dependent isotopic system. Chem Geol 101:123–129. https://doi.org/10.1016/0009-2541(92)90209-N

Qian JZ, Tong Y, Ma L, Zhao WD, Zhang RG, He XR (2017) Hydrochemical characteristics and groundwater source identification of a multiple aquifer system in a coal mine. Int J Mine Water 37:528–540. https://doi.org/10.1007/s10230-017-0493-x

Qin WJ, Han DM, Song XF, Liu SH (2021) Environmental isotope (δ^{18}O, δ^2H, ^{222}Rn) and hydrochemical evidence for understanding rainfall-surface water-groundwater transformations in a polluted karst area. J Hydrology 592:125748. https://doi.org/10.1016/j.jhydrol.2020.125748

Ruhl LS, Dwyer GS, Hsu-Kim H, Hower JC, Vengosh A (2014) Boron and strontium isotopic characterization of coal combustion residuals: Validation of new environmental tracers. Environ Sci Technol 48:14790–14798. https://doi.org/10.1021/es503746v

Shan JJ, Zhong XY, Wang XQ, Fan QS, Du YS, Qin ZJ, Shan FS (2018) Research on interpretation for underground water bearing structure of coal mine by transient electromagnetic method: a case study in Dongming open coal mine in Inner Mongolia. J Salt Lake Sci 26(4):27–33 **(in Chinese)**

Silva TR, Lima MMC (2023) Water quality assessment and hydrogeochemistry of a sedimentary basin in a semi-arid area under increasing exploitation: insights from multivariate statistical analyses, GIS, and modeling. Appl Geochem 150:105593. https://doi.org/10.1016/j.apgeochem.2023.105593

Sun CJ, Zhou SJ, Jing ZW (2023) Variability of precipitation-stable isotopes and moisture sources of two typical landforms in the eastern Loess Plateau. China J Hydrol Reg Stud 46:101349. https://doi.org/10.1016/j.ejrh.2023.101349

Tarasenko I, Kholodov AS, Zin'kov A, Chkryzhov I (2022) Chemical composition of groundwater in abandoned coal mines: evidence of hydrogeochemical evolution. Appl Geochem 137:105210. https://doi.org/10.1016/j.apgeochem.2022.105210

Terzer-Wassmuth S, Wassenaar LI, Welker JM, Araguás-Araguás L (2021) Improved high-resolution global and regionalized isoscapes of δ^{18}O, δ^2H and d-excess in precipitation. Hydrol Process 35:e14254. https://doi.org/10.1002/hyp.14254

Vengosh A, Starinsky A, Kolodny Y, Chivas AR, Raab M (1992) Boron isotope variations during fractional evaporation of sea water: new constraints on the marine versus nonmarine debate. Geology 20:799–802. https://doi.org/10.1130/0091-7613(1992)020%3c0799:BIVDFE%3e2.3.CO;2

Wan CB (2006) Cretaceous palynological flora in Hailar Basin. Jilin Univ (in Chinese), PhD Diss

Williams LB, Hervig RL (2004) Boron isotope composition of coals: a potential tracer of organic contaminated fluids. Appl Geochem 19:1625–1636. https://doi.org/10.1016/j.apgeochem.2004.02.007

Wu Q, Mu WP, Xing Y, Qian C, Shen JJ, Wang Y, Zhao DK (2017) Source discrimination of mine water inrush using multiple methods: a case study from the Beiyangzhuang Mine, northern China. B Eng Geol Environ 3:1–14. https://doi.org/10.1007/s10064-017-1194-1

Xiao J, Xiao YK, Jin ZD, He MY, Liu CQ (2013) Boron isotope variations and its geochemical application in nature. Aust J Earth Sci 60(4):431–447. https://doi.org/10.1080/08120099.2013.813585

Xiao YK, Wang L (2001) The effect of pH and temperature on the isotopic fractionation of boron between saline brine and sediments. Chem Geol 171:253–261. https://doi.org/10.1016/S0009-2541(00)00251-5

Yang ZY, Huang PH, Ding FF (2020) Groundwater hydrogeochemical mechanisms and the connectivity of multilayer aquifers in a coal mining region. Mine Water Environ 39:808–822. https://doi.org/10.1007/s10230-020-00716-4

Zhang HT, Xu GQ, Zhan HB, Chen XQ, Liu MC, Wang MH (2020a) Identification of hydrogeochemical processes and transport paths of a multi-aquifer system in closed mining regions. J Hydrology 589:125344. https://doi.org/10.1016/j.jhydrol.2020.125344

Zhang J, Chen HS, Fu ZY, Wang F, Wang KL (2023) Towards hydrological connectivity in the karst hillslope critical zone: insight from using water isotope signals. J Hydrology 617:128926. https://doi.org/10.1016/j.jhydrol.2022.128926

Zhang J, Chen LW, Chen YF, Ge RT, Ma L, Zhou KD, Shi XP (2020b) Discrimination of water-inrush source and evolution analysis of hydrochemical environment under mining in Renlou coal mine, Anhui Province, China. Environ Earth Sci 39:808–822. https://doi.org/10.1007/s12665-019-8803-1

Zhang L, Chen ZY, Liu FL, Jia YK, Zhang XY, Chen L (2011) Study on methods for hydrogen and oxygen isotope analysis of water samples. Rock Miner Anal 30(2):160–163 **(in Chinese)**

Zhang XL, Luo X, Jiao JJ, Li HL, Lian EG, Yang SY, Kong FC, Kuang XX, Zuo JC (2021) Hydrogeochemistry and fractionation of boron isotopes in the inter-dune aquifer system of Badain Jaran Desert. China J Hydrol 595:125984. https://doi.org/10.1016/j.jhydrol.2021.125984

Zhang Y, Tan HB, Cong PX, Rao WB, Ta WQ, Lu SC, Shi DP (2022) Boron and lithium isotopic constraints on their origin, evolution, and enrichment processes in a river-groundwater-salt lake system in the Qaidam Basin, northeastern Tibetan Plateau. Ore Geol Rev 149:105110. https://doi.org/10.1016/j.oregeorev.2022.105110

Zhao KD, Jiang SY, Nakamura E, Moriguit T, Wei HZ (2015) A preliminary study on boron isotope fractionation of major rock-forming minerals in granite. Acta Petrol Sin 31:740–746

Zhao L, Ting R, Wang NB (2017) Groundwater impact of open cut coal mine and an assessment methodology: a case study in NSW. Int J Min Sci Techn 27:861–866. https://doi.org/10.1016/j.ijmst.2017.07.008

Zhao X, Peng WH, Chen K, Qiu XY, Sun LH (2022) Potential hydraulic connectivity of coal mine aquifers based on statistical analysis

of hydrogeochemistry. Water Sci Eng 15(4):285–293. https://doi.org/10.1016/j.wse.2022.08.004

Zheng XY, Lv YP (1994) The natural environment of the formation of Hailar Basin. J Salt Lake Sci 2(3):10–16 **(in Chinese)**

Zheng XY, Lv YP (1995) Salt lakes and carbonate origin in Hailar Basin. J Salt Lake Sci 3(3):1–10 **(in Chinese)**

Zheng ZX, Zhang Y, Li BY (2023) Sensitivity assessment of boron isotope as indicator of contaminated groundwater for hydraulic fracturing flowback fluids produced from the Dameigou shale of the northern Qaidam Basin. Sustainability 15:5481. https://doi.org/10.3390/su15065481